Progress In Electromagnetics Research, PIER 43, 305–333, 2003

SCATTERING BY PARALLEL CYLINDRICAL POSTS WITH CONDUCTING STRIPS

R. Lech, M. Polewski, and J. Mazur

Department of Electronics, Telecommunications and Informatics
Gdańsk University of Technology (GUT)
11/12 Narutowicza str., Gdańsk 80-952, Poland

Abstract—The theory of scattering in open and closed areas by a novel structure of a dielectric-metallic post is developed with the use of a combination of a modified iterative scattering procedure and an orthogonal expansion method. The scattered field pattern for open structures and frequency responses of the transmission and re ection coefficients in a rectangular waveguide are derived. The turn and displacement of the post in a waveguide allows to change the resonance frequency of the circuit. A good agreement is obtained between the results of our method and those received from FDTD simulations and measurements. The proposed model is much faster than the FDTD method used for comparison. The computation time is independent of the kind of dielectric material the post is made of.

1. INTRODUCTION

For decades the dielectric and metallic resonators have been extensively investigated for applications in microwave communication systems [1–10]. Numerous different methods of analysis are used to examine the resonators depending on their shapes and type of excitation. For plane wave scattering, where the posts are in free space, one can distinguish several developed techniques such as partial differential equation with the eigenfunction expansion method [3], integral equation formulation, [4] and the iterative algorithm [6]. For waveguide structures one can mention the modal expansion method [5] and the orthogonal expansion method [8, 9].

In recent years the space-discretization techniques such as FDTD or FEM employed in professional simulators have become more popular thus enabling to investigate the structures with arbitrary cross section or profile. Nevertheless, these techniques are not very efficient, considering the time of analysis for the structures with high complexity where extremely fine discretization is needed. In this paper we would like to show the analytical solution for the dielectric-metallic cylindrical obstacles with complex shapes.

The mathematical model from [1] and [2] based on a combination of an iterative scattering procedure and an orthogonal expansion method [6–10] is modified on the investigated structures. The proposed procedure enables to analyze the electromagnetic wave scattering of TE waves from two-dimensional posts in both open and closed structures. In the former the posts are placed in free space and the far scattered field patterns are investigated. For the latter the frequency responses of the transmission and re ection coefficients in a rectangular waveguide describing the resonances of the posts on the dominant waveguide mode are derived. For both problems the cylindrical interaction region is

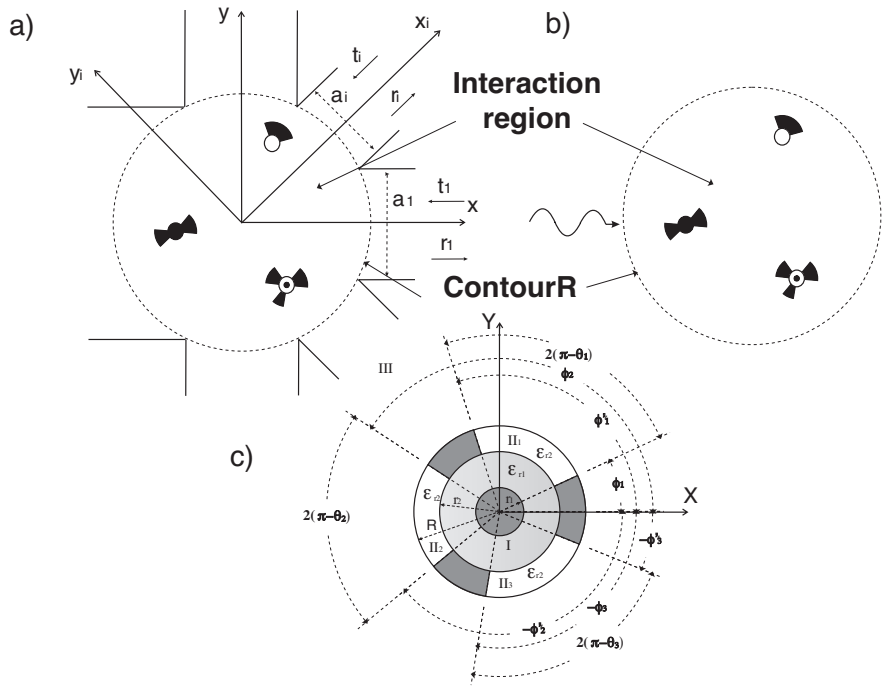

Figure 1. Schematic representation of the scattering by cylindrical posts with metallic strips in a) waveguide junction, b) open area; c) single post in local coordinate system.

separated (see. Fig. 1) where a total scattered field from all posts is found. The analysis of scattering of TM waves can be perform analogously but different boundary conditions and basis functions have to be considered. The methodology presented in this paper can be easily developed into circular waveguides and resonators containing dielectric rod with metallic strips.

The investigated cylindrical structure consists of one, two or three conducting strips with finite thickness attached to the central dielectric or conducting cylinder as shown in Fig. 1.

As distinct from common cylindrical dielectric resonators, the investigated structure enables to vary the resonant frequency of the waveguide structure and scattered field by simple rotation of the post. This effect is especially useful in closed structures where it can be used in filter structures to tune a circuit to the demanded frequency. The tuning feature can also correct the resonance frequency resulting from the defects or improper dimensions of the dielectrical resonators. In

order to analyze the considered structure the procedure in [1] should be modified by applying the scattered field found from a single bow-tie post. Then it allows to obtain the multimodal scattering matrix for the considered waveguide structures.

The theory of scattering in open and closed areas by the posts and the description of the fields in a local coordinate system of the single post are reviewed in Section 2. The estimation of numerical error with the convergence of scattering parameters are described in Section 3. The method is verified with the calculation of FDTD simulator for several plane wave scattering configurations and waveguide structures where the comparison with measurement was also carried out. The results on the computation of the radiation patterns and scattering parameters are presented in Section 4. Additionally, the theory and analysis of propagation in periodically loaded waveguide, as an application of investigated structures, are described in Section 4.2.

2. THEORY

The procedure assumes that the posts are excited by an unknown incident field defined as an infinite series of Bessel functions of the first kind with unknown coefficients a_n. A total scattered field from all posts in interaction region on contour R is determined by these unknown coefficients. This approach allows to match the obtained total scattered field with other known incident fields and to define a scattering matrix of the considered structure.

Incident electric field E_z excites a number of posts and therefore it has to be defined in their local coordinates. For the ith post the electric field has the form

$$E_{zi}^{inc(0)} = \sum_{m=-\infty}^{\infty} a_m \sum_{p=-\infty}^{\infty} J_p(k_0 r_i) e^{jp\phi_i} \cdot J_{p-m}(k_0 d_{io}) e^{j(m-p)\phi_{io}} \quad (1)$$

where d_{io} and ϕ_{io} are the distance and the angle between the center of local and global coordinate system.

The scattered and transmitted field components for the ith post are also described as a series of Bessel functions with unknown coefficients b_m (Region III in Fig. 1) for the scattered field, and c_n and c'_n for the transmitted field in Region II:

$$E_{zi}^{s(0)} = \sum_{m=-\infty}^{\infty} b_{im} H_m^{(2)}(k_0\rho) e^{jm\phi} \quad (2)$$

$$E_z^{t(0)}(\rho, \phi_i) = \sum_{n=1}^{\infty} \left(c_n^j J_{l_j}(k_i\rho) + c_n^{j'} Y_{l_j}(k_i\rho) \right) \sin\left(\frac{n\pi(\phi_i - \phi_{j,i})}{2(\pi - \theta_{j,i})} \right) \quad (3)$$

where $H_m^{(2)}$ is a Hankel function of the second kind of order m, J_{l_j} and Y_{l_j} are Bessel functions of the first and second kind, respectively, of order l_j, $l_j = n\pi/2(\pi - \theta_j)$, $j = 1, 2$ and $k_i = k_0\sqrt{\varepsilon_{ri}}$.

Applying the continuity of the tangential components of electric and magnetic fields on the surface of each contour R_i, and using the orthogonalization method, the unknown coefficients b_m are obtained. Truncating the series expansion to $m = M$ the solution is expressed as

$$[b] = [G][T_{io}][a] \tag{4}$$

where $[b]$ and $[a]$ are vectors of the length $(2M + 1)$, $[G]$ is a relation matrix between the unknown coefficients b_m and a_m, and $[T_{io}]$ is the transformation matrix of Bessel functions from global coordinates to the local coordinates of the ith post [2].

Following the procedure described in [2, 6] the total electric and magnetic fields on the surface of the interaction region are determined and described by matrix $[Z]$ in equation (5).

$$\left[E_z^T\right] = [Z]\left[H_\phi^T\right] \tag{5}$$

2.1. Scattering Fields

The scattered field from the investigated obstacles described on the surface of a separated interaction region can be combined with fields of closed and open external structure.

For the waveguide structures the electromagnetic field in the analysis is assumed to be independent of z and therefore, all fields are depicted as TE_{n0} waves, having field components E_z, H_ϕ and H_ρ.

The electric field components E_z^i of the TE_{n0} modes for ith waveguide port in its local Cartesian coordinate system $(x_i,\ y_i,\ z_i)$ is written as follows

$$E_z^i = \sqrt{\frac{2}{a_i b}} \sum_{n=1}^{N} \sin\left[\frac{n\pi}{a_i}\left(y_i + \frac{a_i}{2}\right)\right]\left(t_n^i e^{jk_{xn}^i x_i} + r_n^i e^{-jk_{xn}^i x_i}\right) \tag{6}$$

where t_n^i, r_n^i are the transmission and re ection coefficients, respectively, $k_{xn}^i = \sqrt{\omega^2\epsilon_0\mu_0 - \left(\frac{n\pi}{a_i}\right)^2}$, $i = 1, 2, \ldots, K$ and K denotes the number of waveguide ports. The magnetic fields H_x^i, H_y^i can be determined from E_z^i.

For the open problem the total electric incident field is composed of I TM waves from any ϕ direction. The excitation is assumed to

be located along the negative x-axis at a contour R and shifted by an angle θ_{oi}:

$$E_z^i = \sum_{i=1}^{I} E_{oi} \sum_{n=-\infty}^{\infty} j^{-n} J_n(k_0 R) e^{(jn(\phi-\theta_{oi}))} \tag{7}$$

In both cases the scattered field at a distance ρ from the investigated configuration of posts is defined as

$$E_z^s = \sum_{n=-\infty}^{\infty} r_n H_n^{(2)}(k_0\rho) e^{(jn\phi)} \tag{8}$$

As a result of matching outer excitation fields with those obtained from interaction region on the surface of the hypothetical cylindrical boundary ($\rho = R$) [1, 2] the modal scattering matrix of the investigated waveguide structure is defined in equation (9) and the scattered coefficients for the open structure can be determined from equation (10).

$$[S] = \left(\left[K_w^{ER}\right] - [Z]\left[K_w^{HR}\right]\right)^{-1}\left([Z]\left[K_w^{HT}\right] - \left[K_w^{ET}\right]\right) \tag{9}$$

where $[K_w^{ET}]$, $[K_w^{ER}]$, $[K_w^{HT}]$, $[K_w^{HR}]$, are square matrices of the size $(2M + 1)$ (M — the number of eigenfunctions in the cylindrical interaction region) described in [2].

$$[r] = \left(\left[K_f^{ER}\right] - [Z]\left[K_f^{HR}\right]\right)^{-1}\left([Z]\left[K_f^{HT}\right] - \left[K_f^{ET}\right]\right) \tag{10}$$

where the $[K_f^{ET}]$, $[K_f^{HT}]$ are vectors of the length $(2N + 1)$, $[K_f^{ER}]$ and $[K_f^{HR}]$ are square matrices of the size $(2N + 1)$ described in [2] by equations (34) and (35).

2.2. Single Post in Local Coordinate System

In the case where a dielectric cylinder with a conducting rod is used as the central cylinder of the structure, the axial component of the electric field E_z^I in Region I from Fig. 1 is described as follows

$$E_z^I(\rho,\phi) = \sum_{m=-\infty}^{\infty} g_m \left(J_m(k_1\rho) - \frac{J_m(k_1 r_1)}{Ym(k_1 r_1)} Y_m(k_1\rho)\right) e^{jm\phi} \tag{11}$$

where J_m is Bessel function of the first kind of order m, g_m is an unknown coefficient and $k_1 = k_0\sqrt{\varepsilon_{r1}}$. In Region II the axial components of the electric field are described by (12).

$$E_z^{II_i}(\rho,\phi) = \sum_{n=1}^{\infty}\left(c_n^i J_{l_i}(k_2\rho) + c_n^{i'} Y_{l_i}(k_2\rho)\right)\sin\left(\frac{n\pi(\phi-\phi_i)}{2(\pi-\theta_i)}\right) \qquad (12)$$

where for ith subregion ($i = 1,2,3$) of Region II J_{l_i} and Y_{l_i} are Bessel functions of the first and second kind respectively of order l_i, $l_i = n\pi/2(\pi-\theta_i)$ and c_n^i, $c_n^{i'}$ are unknown coefficients, and $k_2 = k_0\sqrt{\varepsilon_{r2}}$.

In the external Region III the electric field has the form:

$$E_z^{III}(\rho,\phi) = \sum_{m=-\infty}^{\infty}\left(a_m J_m(k_0\rho) + b_m H_m^{(2)}(k_0\rho)\right)e^{jm\phi} \qquad (13)$$

where J_m and $H_m^{(2)}$ are Bessel and Hankel functions of order m, and a_m, b_m are unknown coefficients.

For further numerical investigation the numbers of harmonics $n = 1 \ldots N$ for the fields (12), and $m = -M \ldots M$ for the fields (11) and (13) are taken into account. In order to modify the model in [1] it is necessary to find the novel relation between the unknown coefficients a_m and b_m defined in equation (13). Hence, the boundary conditions at the interfaces I–II$_i$ ($\rho = r_2$) and II$_i$-III ($\rho = R$) should be satisfied. The tangential component E_z of electric fields is assumed as an unknown function $U^{(i)}(\phi)$, leading to the following relations:

$$U^{(i)}(\phi) = \begin{cases} 0, & \phi_i' \le \phi \le 2\pi + \phi_i \\ E_z^I(\rho = r_2,\phi) = E_z^{II_i}(\rho = r_2,\phi), & \phi_i \le \phi \le \phi_i' \\ E_z^{II_i}(\rho = R,\phi) = E_z^{III}(\rho = R,\phi), & \phi_i \le \phi \le \phi_i' \end{cases} \qquad (14)$$

Expanding function $U^{(i)}(\phi)$ in a series of basis functions with unknown coefficients $w_k^{(i)}$ and assuming the number of terms in expansion K one gets:

$$U^{(i)}(\phi) = \sum_{k=1}^{K} w_k^{(i)} U_k^{(i)}(\phi), \qquad i = 1,2 \qquad (15)$$

A set of basis functions satisfying the conditions at the sharp metallic edges of the ridge is taken from [11] and described by (16).

$$U_k^{(i)}(\phi) = \frac{\sin\left[\dfrac{k\pi(\phi-\phi_i)}{2(\pi-\theta_i)}\right]}{\sqrt[3]{(\phi-\phi_i)\left[2(\pi-\theta_i)-(\phi-\phi_i)\right]}} \qquad (16)$$

for $i = 1, 2, 3$.

Additional relations between the H_ϕ fields at the interface ($\rho = r_2$) and ($\rho = R$) are obtained:

$$H_\phi^I(\rho = r_2, \phi) = H_\phi^{II_i}(\rho = r_2, \phi), \quad \phi_i \le \phi \le \phi_i' \tag{17}$$

$$H_\phi^{II_i}(\rho = R, \phi) = H_\phi^{III}(\rho = R, \phi), \quad \phi_i \le \phi \le \phi_i' \tag{18}$$

Substituting the boundary conditions (14) and (17) to the fields (11) and (12), and using field eigenfunctions $\{e^{-jm\phi}\}$ and $\left\{ \sin\left(\frac{n\pi(\phi-\phi_i)}{2(\pi-\theta_i)}\right)\right\}$ to orthogonalize (11) and (12) respectively, the coefficient g_m is eliminated and the following relations between coefficients $c_m^{i'}$ and c_m^i can be received:

$$\begin{bmatrix} \mathbf{c^{1'}} \\ \mathbf{c^{2'}} \\ \mathbf{c^{3'}} \end{bmatrix} = \begin{bmatrix} \mathbf{M_{11}} & \mathbf{M_{12}} & \mathbf{M_{13}} \\ \mathbf{M_{21}} & \mathbf{M_{22}} & \mathbf{M_{23}} \\ \mathbf{M_{31}} & \mathbf{M_{32}} & \mathbf{M_{33}} \end{bmatrix} \begin{bmatrix} \mathbf{c^1} \\ \mathbf{c^2} \\ \mathbf{c^3} \end{bmatrix} \tag{19}$$

where $\mathbf{c^i}$ and $\mathbf{c^{i'}}$ are the vectors of the length N. The matrices $\mathbf{M_{ij}}$ for $i,\ j = 1, 2, 3$ are square of dimension $N \times N$ and for dielectric and conducting cylinder are defined in the Appendix. Applying the relations (19) to the fields (12), and then making use of the orthogonality of field eigenfunctions at the boundary conditions (14) at the interface ($\rho = R$), the following set of equations is obtained,

$$\begin{bmatrix} \mathbf{c^1} \\ \mathbf{c^2} \\ \mathbf{c^3} \\ \mathbf{c^{1'}} \\ \mathbf{c^{2'}} \\ \mathbf{c^{3'}} \end{bmatrix} = \begin{bmatrix} \mathbf{P_{11}} & \mathbf{P_{12}} & \mathbf{P_{13}} \\ \mathbf{P_{21}} & \mathbf{P_{22}} & \mathbf{P_{23}} \\ \mathbf{P_{31}} & \mathbf{P_{32}} & \mathbf{P_{33}} \\ \mathbf{W_{11}} & \mathbf{W_{12}} & \mathbf{W_{13}} \\ \mathbf{W_{21}} & \mathbf{W_{22}} & \mathbf{W_{23}} \\ \mathbf{W_{31}} & \mathbf{W_{32}} & \mathbf{W_{33}} \end{bmatrix} \begin{bmatrix} \mathbf{w^{(1)}} \\ \mathbf{w^{(2)}} \\ \mathbf{w^{(3)}} \end{bmatrix} \tag{20}$$

together with the equation defining the coefficients $\mathbf{a}$ versus $\mathbf{w^{(i)}}$ and $\mathbf{b}$:

$$\mathbf{a} = \mathbf{Q_1 w^{(1)}} + \mathbf{Q_2 w^{(2)}} + \mathbf{Q_3 w^{(3)}} - \mathbf{Q_4 b} \tag{21}$$

where the dimensions of matrices $\mathbf{P_{ij}}$, $\mathbf{W_{ij}}$ for $i,\ j = 1, 2, 3$ are $N \times K$, while for matrix $\mathbf{Q_i}$ is $(2M + 1) \times K$ and for matrix $\mathbf{Q_4}$ — $(2M + 1) \times (2M + 1)$. All the above-mentioned matrices are presented in the Appendix by equations (A4)–(A7). The vectors $\mathbf{a}$ and $\mathbf{b}$ are of the length $2M + 1$, and $\mathbf{w^{(i)}}$ are of the length K.

With the above results the boundary conditions (18) are now considered. Having orthogonalized them using base functions as weight functions, the following set of equations is received

$$\begin{aligned}&\mathbf{U^{0(i)T}J'_{l_i}(k_2R)c^i} + \mathbf{U^{0(i)T}Y'_{l_i}(k_2R)c^{i'}} + \\ &-\mathbf{U^{\phi 0(i)T*}}\left(\mathbf{J'_m(k_0R)a} + \mathbf{H_m^{(2)'}(k_0R)b}\right) = 0\end{aligned} \tag{22}$$

where the matrices $\mathbf{U^{0(i)}}$, $\mathbf{U^{\phi(i)}}$ are of the dimension $N \times K$ and $(2M+1) \times K$, respectively, and are defined by equations (A2) and (A3). $\mathbf{J_{l_i}}$, $\mathbf{Y_{l_i}}$ and $\mathbf{J_m}$, $\mathbf{H_m^{(2)}}$ for $i = 1, 2, 3$ are diagonal matrices of the dimension $N \times N$ and $(2M+1) \times (2M+1)$, respectively. Applying (20) and (21) to (22) the vector coefficients $\mathbf{w^{(i)}}$ are determined as follows:

$$\mathbf{w^{(i)}} = \mathbf{L^i} \cdot \mathbf{b} \tag{23}$$

where the matrices $\mathbf{L^i}$ are presented in the Appendix.

Substituting (23) to (21) after some algebra, the demanded relation between unknown coefficients a_m and b_m is obtained:

$$\mathbf{b} = \mathbf{F^{-1}a} = \mathbf{G} \cdot \mathbf{a} \tag{24}$$

where

$$\mathbf{F}_{pq} = \begin{cases} \dfrac{1}{J_p(k_0R)} \displaystyle\sum_{i=1}^{3}\sum_{k=1}^{K}\left(U_{k,p}^{\phi(i)} L_{k,p}^{i}\right) - \dfrac{H_p^{(2)}(k_0R)}{J_p(k_0R)} & \text{for} \quad p = q \\ \dfrac{1}{J_p(k_0R)} \displaystyle\sum_{i=1}^{3}\sum_{k=1}^{K}\left(U_{k,p}^{\phi(i)} L_{k,p}^{i}\right) & \text{for} \quad p \neq q \end{cases} \tag{25}$$

for $p, q = -M, \ldots, -1, 0, 1, \ldots, M$.

Introducing equation (24) to equation (8) in the mathematical model presented in [1] the relation between the electric and magnetic field on the cylindrical surface described on the post is obtained. This relation is essential to calculate the modal scattering matrix of the circuit as used in [1].

3. ESTIMATION OF NUMERICAL ERROR

All calculations were conducted on Matlab , 2000+ Athlon (1666-MHz) personal computer (PC).

The precise investigation of the convergence of plane waves for different radii R of interaction region was conducted in [2]. It was

Table 1. Comparison of the percentage error δ_{S11}^{N} for the single post configuration from Fig. 8.

		M = 4	5	6	7	8	9
K = 3	δ[%]	2,295	-0,516	1,596	1,869	0,320	-0,033
4	δ[%]	2,399	-0,243	1,721	1,717	0,132	-0,150
5	δ[%]	2,416	-0,239	1,619	1,445	-0,085	-0,018
6	δ[%]	2,418	-0,216	1,614	1,447	-0,048	0,070
7	δ[%]	2,426	-0,213	1,603	1,437	-0,048	0,066
8	δ[%]	-70,49	-0,213	1,599	1,436	-0,041	0,074
9	δ[%]	20,27	-0,213	1,600	1,437	-0,044	0,077
10	δ[%]	4,925	-73,55	1,592	1,436	-0,041	0,081
11	δ[%]	45,38	-41,95	1,592	1,437	-0,041	0,081

concluded that while increasing the radius R, the number of harmonic functions should also be increased to describe an excitation with the required error.

For the structure investigated in this paper it is necessary to show the estimation of numerical error for the scattering coefficients assuming various number of eigenfunctions N and basis functions K. It is convenient to use the waveguide structure where the convergence of $|S_{11}|$, $|S_{21}|$ for the fundamental mode can be shown for selected configuration of the posts. In order to examine the convergence of the solution the following error criteria are defined:

$$\delta_{S11}^{N}[\%] = \frac{\left|S_{11}^{N}\right| - \left|S_{11}^{N-1}\right|}{\left|S_{11}^{N}\right|} \quad \delta_{S11}^{K}[\%] = \frac{\left|S_{11}^{K}\right| - \left|S_{11}^{K-1}\right|}{\left|S_{11}^{K}\right|}$$

$$\delta_{S21}^{N}[\%] = \frac{\left|S_{21}^{N}\right| - \left|S_{21}^{N-1}\right|}{\left|S_{21}^{N}\right|} \quad \delta_{S21}^{K}[\%] = \frac{\left|S_{21}^{K}\right| - \left|S_{21}^{K-1}\right|}{\left|S_{21}^{K}\right|}$$

As an example the configuration of a single post presented in Fig. 8 is analyzed to show the effect of obtaining convergence for $|S_{11}|$ and $|S_{21}|$. The parameters of the investigated configuration: $r_1 = 1.5\,\mathrm{mm}$, $R = 5\,\mathrm{mm}$, $\Delta\phi_{1,2} = 30^\circ$, $d = 5\,\mathrm{mm}$; $f = 12.25\,\mathrm{GHz}$. The results are presented in Tables 1, 2, 3 and 4.

From the results one can observe the correlation between the expansion numbers of eigenfunctions and basis functions. The choice of the basis function number K is limited by the chosen number of eigenfunctions $N = 2M + 1$. If their ratio K/N is bigger than one, the error increases rapidly. It is also worth noticing that the choice

Table 2. Comparison of the percentage error δ_{S11}^{K} for the single post configuration from Fig. 8.

		K = 4	5	6	7	8	9	10	11
M = 3	δ[%]	0,307	-0,093	0,066	-0,027	42,78	-113,8	51,58	-112,8
4	δ[%]	0,413	-0,076	0,068	-0,019	0,027	-0,008	42,26	-22,26
5	δ[%]	0,684	-0,072	0,091	-0,015	0,027	-0,008	0,015	-0,004
6	δ[%]	0,810	-0,176	0,086	-0,026	0,022	-0,007	0,007	-0,004
7	δ[%]	0,657	-0,453	0,088	-0,037	0,022	-0,007	0,007	-0,004
8	δ[%]	0,469	-0,671	0,125	-0,037	0,029	-0,011	0,011	-0,004
9	δ[%]	0,352	-0,539	0,214	-0,041	0,037	-0,007	0,015	-0,004

Table 3. Comparison of the percentage error δ_{S21}^{N} for the single post configuration from Fig. 8.

		M = 4	5	6	7	8	9
K = 3	δ[%]	-0,535	0,110	-0,129	-0,131	-0,019	0,003
4	δ[%]	-0,544	0,089	-0,140	-0,122	-0,003	0,012
5	δ[%]	-0,545	0,090	-0,133	-0,099	0,014	0,002
6	δ[%]	-0,546	0,088	-0,133	-0,099	0,011	-0,005
7	δ[%]	-0,547	0,088	-0,131	-0,099	0,011	-0,005
8	δ[%]	7,168	0,088	-0,131	-0,099	0,010	-0,005
9	δ[%]	-1,487	0,088	-0,132	-0,098	0,010	-0,005
10	δ[%]	-1,203	7,939	-0,131	-0,099	0,010	-0,005
11	δ[%]	-5,954	4,199	-0,131	-0,099	0,010	-0,005

Table 4. Comparison of the percentage error δ_{S21}^{K} for the single post configuration from Fig. 8.

		K = 4	5	6	7	8	9	10	11
M = 3	δ[%]	-0,022	0,006	-0,004	0,002	-8,313	8,529	-8,834	8,214
4	δ[%]	-0,030	0,005	-0,005	0,001	-0,002	0,001	-8,529	3,904
5	δ[%]	-0,051	0,006	-0,007	0,001	-0,002	0,001	-0,001	0,000
6	δ[%]	-0,062	0,013	-0,007	0,003	-0,002	0,000	0,000	0,000
7	δ[%]	-0,053	0,036	-0,007	0,003	-0,002	0,001	-0,001	0,000
8	δ[%]	-0,037	0,053	-0,009	0,003	-0,003	0,001	-0,001	0,000
9	δ[%]	-0,028	0,043	-0,017	0,003	-0,003	0,001	-0,001	0,000

of number of basis function and eigenfunctions is determined by the configuration of the post. To be precise it depends on the angular aperture of the Region II (see Fig. 1) between the metallic strips.

For presented examples it can be assumed that it is sufficient to select the $M = 9$ of eigenfunctions and $K = 9$ of basis functions to obtain a good convergence. It should be pointed out here that for other configurations (not presented in this paper) the number of eigenfunctions and basis functions has to be chosen individually.

The axial components of the electric field in Region II defined by equation (12) strongly depends on the θ_i angle, which determines the angular aperture of this region. For the value of θ_i angle approaching π the order of Bessel functions J_{l_i} and Y_{l_i} defined by

$$l_i = \frac{n\pi}{2(\pi - \theta_i)} \tag{26}$$

increases, causing the value of Bessel functions to decrease. Assuming the chosen number of eigen-functions M and a high value of θ_i angle the numerical precision used in MATLAB is not sufficient for calculation, causing the calculated value of Bessel functions for higher modes (high value of n in equation (26)) to equal zero and resulting in calculation errors.

To overcome those errors one can use the tangential approximations of Bessel functions for high value index [12], or assume the boundary computable value of Bessel function for higher modes. These operations do not introduce any additional errors and let the calculations run.

Table 5 depicts the boundary values of Bessel function, its derivative and their ratio versus frequency for single bow-tie post configuration with $\theta_1 = 17/18\pi$ and $r = 4.5\,\text{mm}$. The last computable value of Bessel function is for $m = 7$; $(n = 2m + 1 = 15)$, which gives $l = 135$.

4. NUMERICAL AND MEASURED RESULTS

In order to check the validity of the presented approach, our simulations of open structures were compared with the calculations of the commercial FDTD simulator Quick Wave 3D [13], and for waveguide structures also with our own measurements.

4.1. Multipost Plane Wave Scattering

A few configurations of the posts with a metallic and a dielectric rod were simulated. Figs. 2 and 3 show the calculations of the scattering by

Table 5. Boundary value of Bessel function $J_l(k_0 r)$ for $l = 135$, $r = 4.5\,\mathrm{mm}$.

f [GHz]	9	9.5	10	10.5	11
$J_l(k_0 r)$	0.1905 ¤10^{-280}	0.2817 ¤10^{-277}	0.2864 ¤10^{-274}	0.2077 ¤10^{-271}	0.1109 ¤10^{-268}
$J_l'(k_0 r)$	0.1364 ¤10^{-280}	0.1911 ¤10^{-277}	0.1846 ¤10^{-274}	0.1275 ¤10^{-271}	0.0650 ¤10^{-268}
J_l'/J_l	0 7162	0 6785	0.6446	0.6139	0.5860
f [GHz]	11 5	12	12:5	13	
$J_l(k_0 r)$	0.4477 ¤10^{-266}	0.1400 ¤10^{-263}	0.3463 ¤10^{-261}	0.6900 ¤10^{-259}	
$J_l'(k_0 r)$	0.2509 ¤10^{-266}	0.0752 ¤10^{-263}	0.1786 ¤10^{-261}	0.3421 ¤10^{-259}	
J_l'/J_l	0.5605	0.5371	0.5156	0.4958	

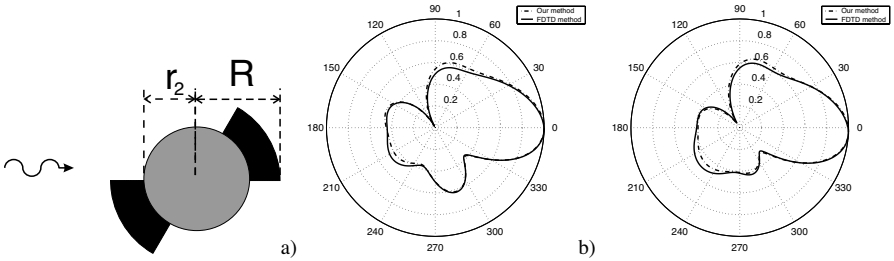

Figure 2. Normalized electric field characteristic for scattering by a single post with a) metallic b) dielectric ($\varepsilon_{r1} = 5$) inner rod. Dimensions of the post are: $r_2 = 3\,\mathrm{mm}$, $R = 10\,\mathrm{mm}$, $\phi_2' = 0°$, $\phi_1 = 60°$, $\phi_1' = 180°$, $\phi_2 = 240°$.

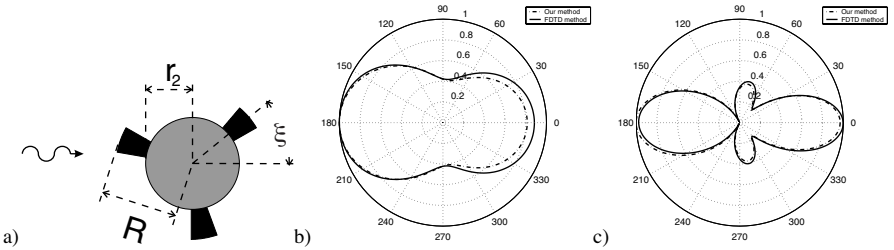

Figure 3. Normalized electric field characteristic for scattering by a single post with dielectric ($\varepsilon_{r1} = 5$) inner rod, for different radius R of the strips. Dimensions of the post are: $r_2 = 3\,\mathrm{mm}$, $\phi_3' = -10°$, $\phi_1 = 10°$, $\phi_1' = 110°$, $\phi_2 = 130°$, $\phi_2' = 230°$, $\phi_3 = 250°$, $\xi = 0°$; b) $R = 4\,\mathrm{mm}$; c) $R = 10\,\mathrm{mm}$.

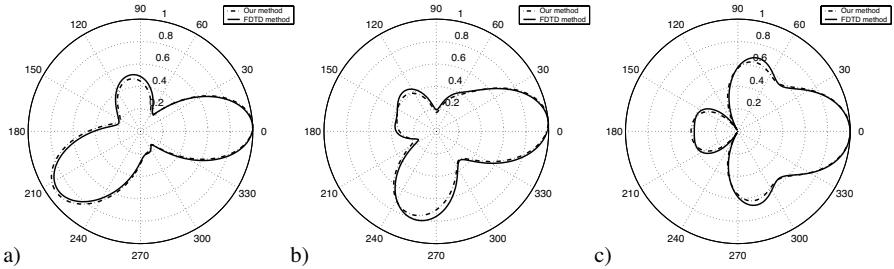

Figure 4. Normalized electric field characteristic for scattering by a single post described in Fig. 3, for several rotation angle ξ. a) $\xi = 20°$, b) $\xi = 40°$, c) $\xi = 60°$.

a single element. Normalized electric field characteristic for scattering by a single post from Fig. 2a is calculated for a metallic post. The characteristic in Fig. 2b is made for the post with dielectric inner rod $\varepsilon_r = 5$. The radius of the rod is $r_2 = 3\,\text{mm}$ and the segments of metallic cylinder $R = 10\,\text{mm}$. The calculations were conducted on frequency $f = 15\,\text{GHz}$. From comparison of the scattering characteristics it is evident that their shapes are similar in both cases, hence the strips have the most significant in uence on the characteristic shape. The results of scattering by a configuration of dielectric post with three strips are presented in Fig. 3, where the in uence of the strips dimensions is clearly evident. As shown in Fig. 4 while turning the post the characteristic is significantly changed, as it was expected. It is worth noticing that our results well agree with those obtained from the FDTD simulations.

In Fig. 5 the plane wave scattering by configurations of four and five posts for two frequencies of excitation wave are presented. One can see that for both frequencies the removal of central post from the investigated array causes the side lobes to appear. A good agreement obtained with the FDTD method calculations proves the correctness of the analysis and verifies the accuracy of the developed computer code.

A scattering by linear arrays of five posts is shown in Fig. 6. As can be seen from the results by adding two metallic strips to each cylinder and rotating the post symmetrically by an angle ξ_1 and ξ_2 one obtains the reduction of the back lobe observed in the previous configurations.

Similar effect concerning the reduction of sidelobs was observed during the investigation of the array of five horizontally placed dielectric posts ($\varepsilon_r = 10$) with three strips (see Fig. 7).

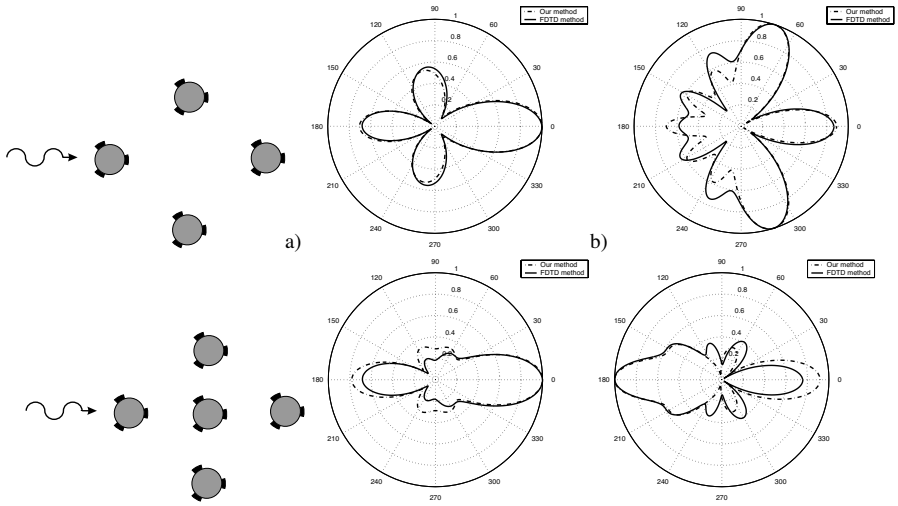

Figure 5. Normalized energy characteristics for scattering by a configuration of four and five posts with dielectric rod ($\varepsilon_r = 5$) for two frequencies a) $f = 15\,\text{GHz}$, b) $f = 20\,\text{GHz}$. The dimensions of the posts are $r_2 = 2\,\text{mm}$, $R = 3\,\text{mm}$. The posts placement: $d_1 = (-10; 0)\,\text{mm}$, $d_2 = (10; 0)\,\text{mm}$, $d_3 = (0; 10)\,\text{mm}$, $d_4 = (0; -10)\,\text{mm}$, $d_5 = (0; 0)\,\text{mm}$.

4.2. Waveguide Structures

The single and double post configurations in WR-90 waveguide were simulated and measured. The experiment was performed using Wiltron 37269A (Network Analyzer). All inserted posts extend the entire height of the waveguide.

Figs. 8–13 show the calculations of the frequency re ection $|S_{11}|$ and transmission $|S_{21}|$ coefficient characteristics for single and double post configurations. The comparison with the measurement (Figs. 8 and 9) and the results obtained from Quick Wave 3D simulator (Figs. 8–11) is presented. As can be seen from these figures a good agreement was obtained with both methods and the measure- ment.

The results for a single post with two strips and conducting rod for several displacements d from the waveguide axis are shown in Fig. 8. As can be seen from this figure, while increasing the distance of the post from the waveguide axis the resonance frequency decreases. Fig. 9 describes the results for displaced post with dielectric central cylinder of $\varepsilon_{r_l} = 28$ with and without the dielectric cylinder of $\varepsilon_{r_u} = 5$ placed at the opposite side of the waveguide. A significant variation of resonance frequency is observed while inserting an additional dielectric resonator.

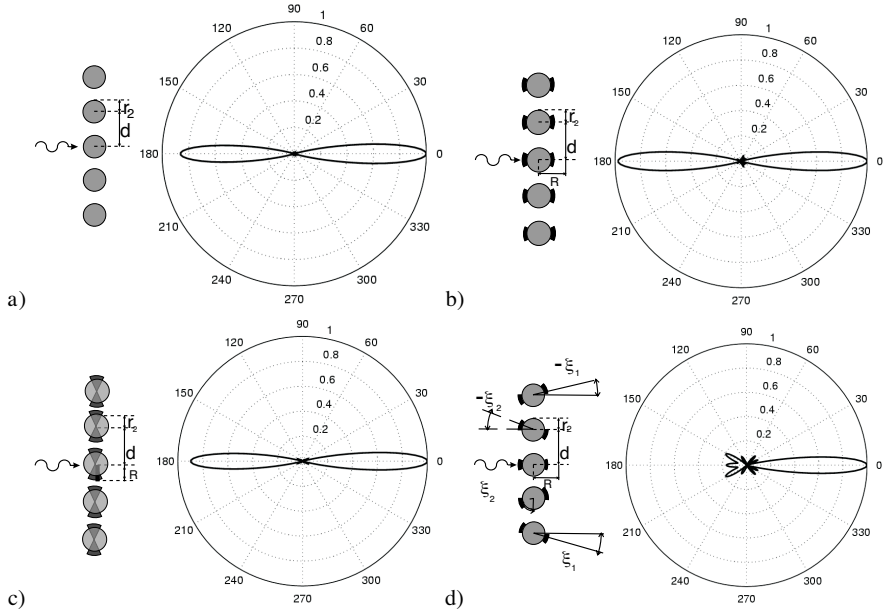

Figure 6. Normalized energy characteristics for scattering by an array of five posts with dielectric rod ($\varepsilon_r = 5$). The dimensions of the posts are $r_2 = 0.1\lambda$, $R = 0.2\lambda$. The distance between the elements is $d = 0.75\lambda$. a) dielectric cylinders; b) dielectric cylinders with horizontally placed metallic strips $\Delta\phi = 12°$; c) 90° rotated post; d) rotated post: $\xi_1 = -42°$, $\xi_2 = 30°$

Fig. 10 presents the re ection coefficients $|S_{11}|$ for the post placed in the center of the waveguide junction for several turn angles ξ. As can be seen, the resonance frequency increases with the increase of the ξ angle. The re ection coefficients $|S_{11}|$ for a configuration of two posts with three strips is shown in Fig. 11. Slight changes of the transmission coefficient $|S_{21}|$ are observed with the turning of the post with three strips as illustrated in Fig. 12. The frequency responses of the post with three strips for two different placements of the strips are described in Fig. 13.

4.2.1. Propagation in Periodically Loaded Waveguide

Having calculated the modal scattering matrix of a single cylindrical section, there is a possibility of using it in a waveguide periodically loaded with investigated post forms. The propagation constants

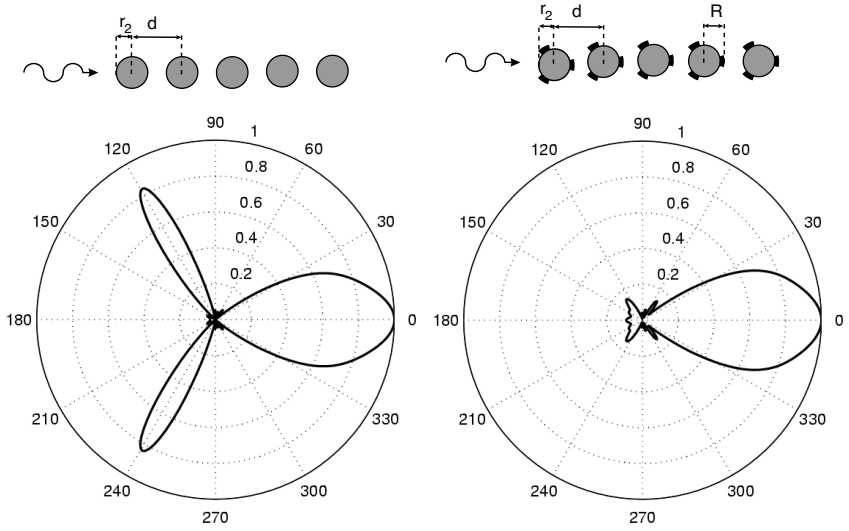

Figure 7. Normalized energy characteristic for scattering by an array of five posts a) dielectric cylinders ($\varepsilon_r 1 = 10$) b) dielectric cylinders with three strips. The dimensions single post is $r_2 = 5\,\text{mm}$, $R = 7\,\text{mm}$. The distance between the elements is $d = 20\,\text{mm}$, $f = 10\,\text{GHz}$.

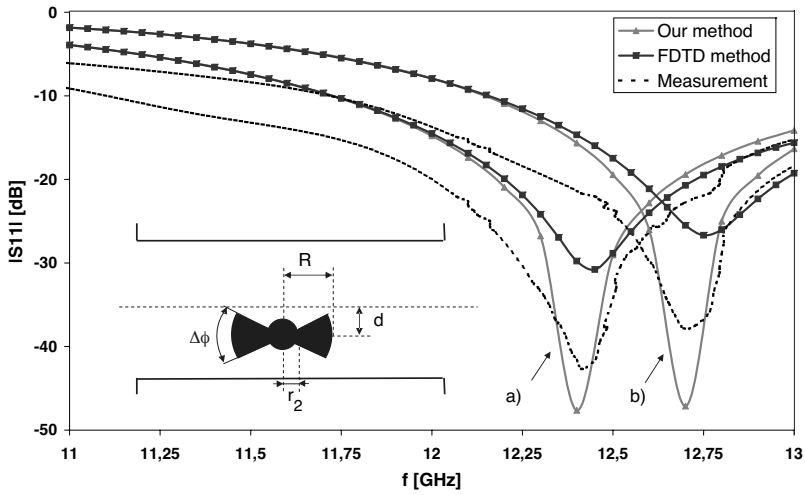

Figure 8. Frequency responses of single metallic post with two strips for the various displacement: $r_2 = 1.5\,\text{mm}$; $R = 5\,\text{mm}$; $\theta = 70°$; angular aperture of the strips is $\Delta\phi = 60°$; $d = 5\,\text{mm}$, $6\,\text{mm}$.

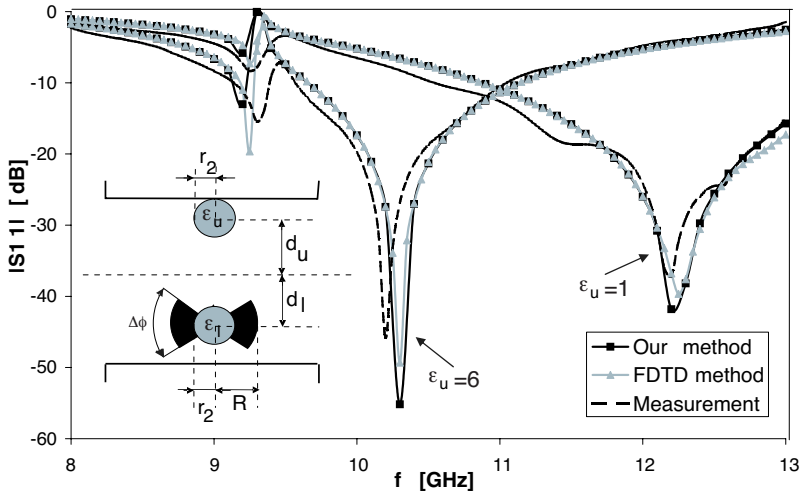

Figure 9. Frequency responses of double post configu- rations: upper post: $r_2 = 2\,\text{mm}$; $\varepsilon_{r_u} = 1$ and 6; lower post: $r_2 = 2\,\text{mm}$; $R = 4\,\text{mm}$; $d_l = -7\,\text{mm}$; $d_u = 9.43\,\text{mm}$; $\varepsilon_{r_l} = 28$; angular aperture of the strips is $\Delta\phi = 42.5°$.

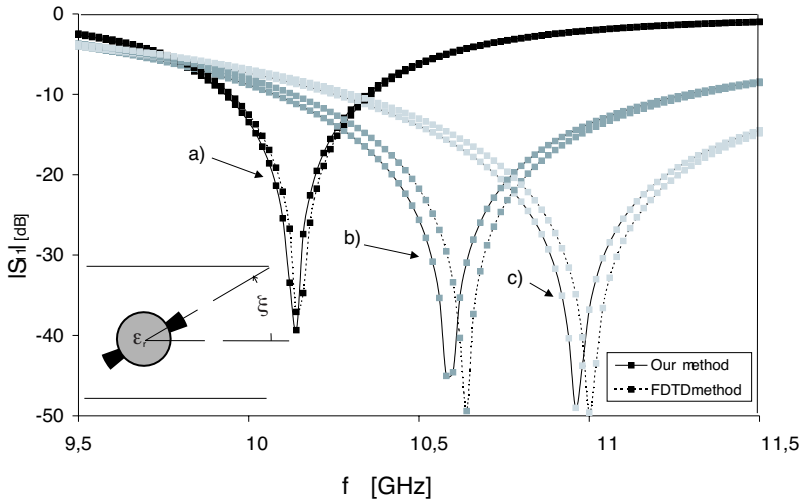

Figure 10. Frequency response of a single post with two conducting strips for the various ξ angle: $r = 3\,\text{mm}$; $R = 4\,\text{mm}$; $\varepsilon = 5$; angular aperture of the strips is $\Delta\phi = 20°$; a) $\xi = 0°$, b) $\xi = 60°$, c) $\xi = 90°$.

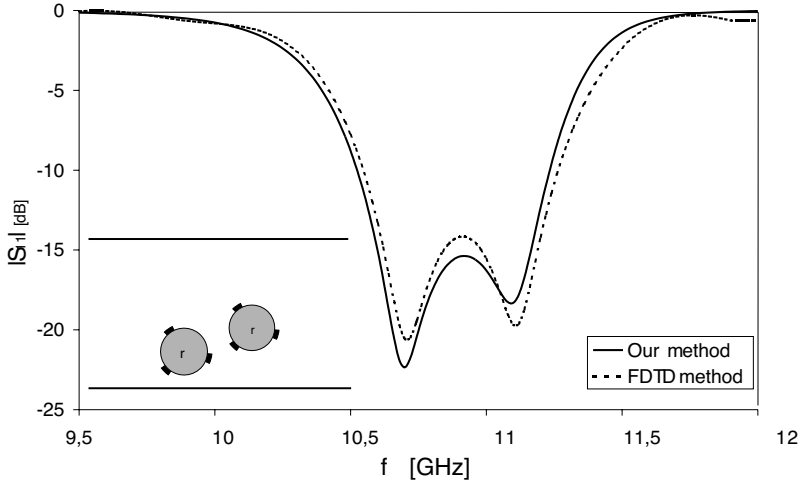

Figure 11. Frequency responses of a double post configuration. The parameters of the posts: $r_i = 3.5\,\text{mm}$; $R_i = 4\,\text{mm}$; $\varepsilon_i = 5$; angular aperture of the strips is $\Delta\phi_i = 22°$, for $i = 1, 2$; $\phi_1^1 = 7°$, $\phi_1^{1'} = 103°$, $\phi_2^1 = 127°$, $\phi_1^{1'} = 228°$, $\phi_3^1 = 252°$, $\phi_3^{1'} = -17°$, $\phi_1^2 = 2°$, $\phi_1^{2'} = 98°$, $\phi_2^2 = 122°$, $\phi_2^{2'} = 223°$, $\phi_3^2 = 247°$, $\phi_3^{2'} = -22°$.

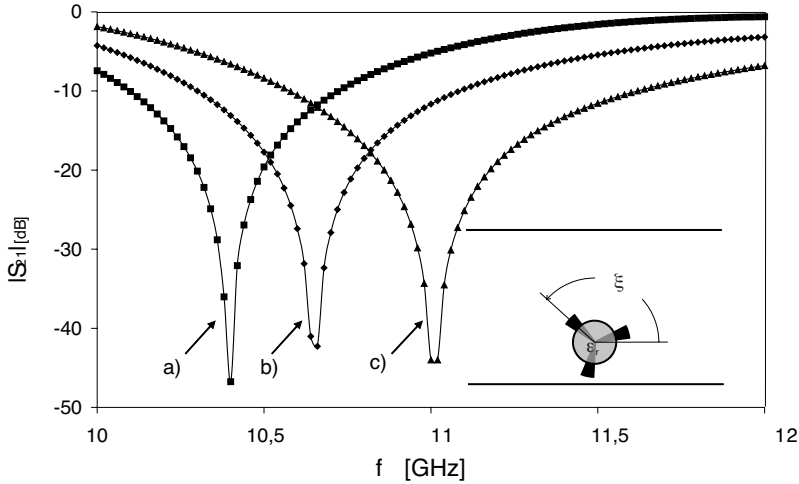

Figure 12. Transmission coefficients of a post with three conducting strips for the various angle ξ: $r = 4\,\text{mm}$; $R = 5\,\text{mm}$; $\varepsilon = 5$; angular aperture of the strips is $\Delta\phi = 20°$; a) $\xi = 140°$, b) $\xi = 120°$, c) $\xi = 90°$.

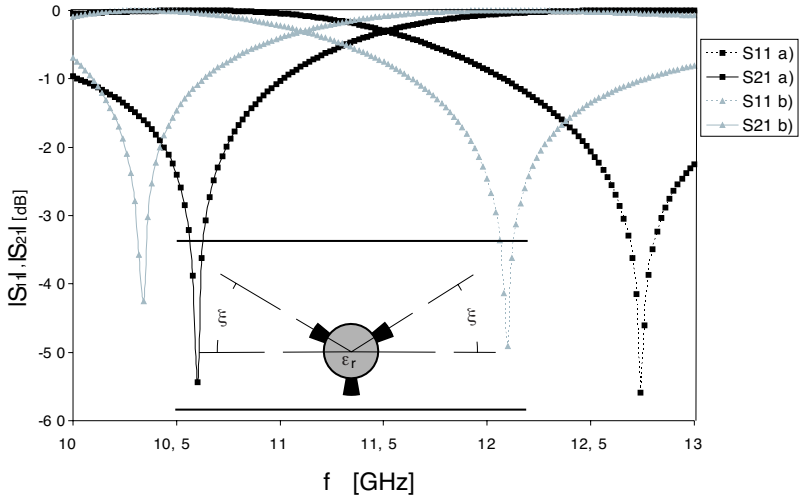

Figure 13. Frequency responses of a post with three conducting strips for the various angle ξ of strips placements: $r = 4\,\mathrm{mm}$; $R = 5\,\mathrm{mm}$; $\varepsilon = 5$; angular aperture of the strips is $\Delta\phi = 20°$; a) $\xi = 0°$, b) $\xi = 30°$.

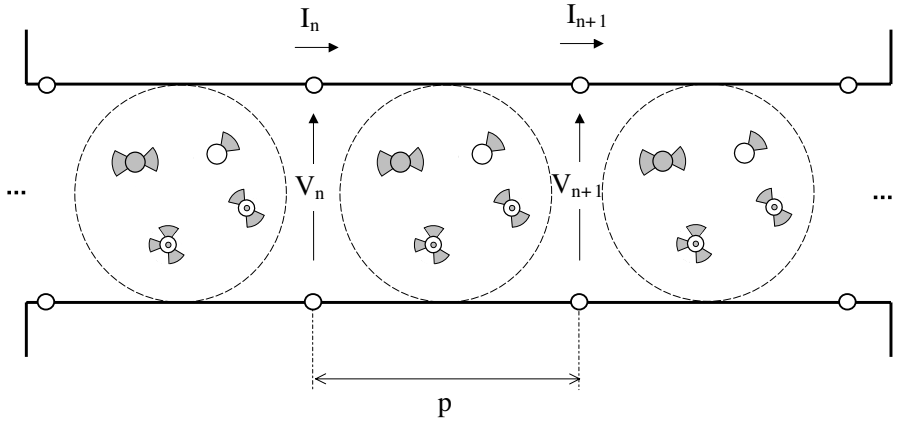

Figure 14. Schematic representation of a waveguide structure periodically loaded by bow-tie cylindrical posts.

of periodic structures will be determined from eigenvalues of a characteristic matrix, as was proposed in [14].

Fig. 14 shows the periodic waveguide structure loaded with investigated posts shapes. The period of the structure is p. The wave is

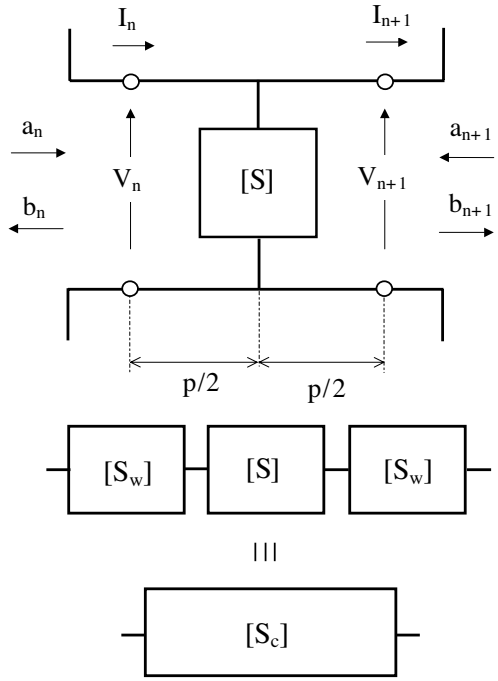

Figure 15. Single periodic section of the length p.

assumed to propagate in the $+z$ direction. For infinitely long structure the Floquet condition describes the connection between adjacent cells. The voltage and current at the nth terminals differ from the voltage and current at the $(n+1)$th terminals by the propagation factor $e^{-\gamma p}$, and can be written as follows

$$\begin{aligned} V_{n+1} &= V_n e^{-\gamma p} \\ I_{n+1} &= I_n e^{-\gamma p} \end{aligned} \tag{27}$$

The scattering matrix of a single periodic section $\mathbf{S^c}$of the length p is calculated as a cascade connection of two segments of the empty waveguide of the length $p/2$ and the previously calculated cylindrical section described by matrix $\mathbf{S}$, as is shown in Fig. 15.

Using the relation (27) the signals a_n, b_n, a_{n+1} and b_{n+1} defining

the scattering matrix of periodic section [Sc] can be written as

$$\begin{aligned} a_n &= V_n + I_n = v \\ b_n &= V_n - I_n = w \\ a_{n+1} &= (V_n - I_n)e^{-\gamma p} = we^{-\gamma p} \\ b_{n+1} &= (V_n + I_n)e^{-\gamma p} = ve^{-\gamma p} \end{aligned} \tag{28}$$

Introducing the above relations to the definition of scattering parameters of a single periodic section one obtains the eigenvalue equation of the form

$$\begin{bmatrix} \mathbf{I} & -\mathbf{S^c_{11}} \\ \mathbf{0} & -\mathbf{S^c_{21}} \end{bmatrix} \begin{bmatrix} \mathbf{w} \\ \mathbf{v} \end{bmatrix} + \lambda \begin{bmatrix} -\mathbf{S^c_{12}} & \mathbf{0} \\ -\mathbf{S^c_{22}} & \mathbf{I} \end{bmatrix} \begin{bmatrix} \mathbf{w} \\ \mathbf{v} \end{bmatrix} = 0 \tag{29}$$

where $\lambda = e^{-\gamma p}$, and γ is the propagation constant. $\mathbf{I}$ is the identity matrix of order $\mathbf{N} \times \mathbf{N}$. $\mathbf{S^c_{11}}$, $\mathbf{S^c_{12}}$, $\mathbf{S^c_{21}}$, and $\mathbf{S^c_{22}}$ are submatrices of order $\mathbf{N} \times \mathbf{N}$ of the modal matrix $\mathbf{S^c}$.

As an example, two periodic structures composed of six sections of a double cylindrical post configuration were analyzed. Figs. 16, 17 represent the plot of propagation constant βp as a function of $k_0 p$ and the frequency responses of the periodic structure. The results illustrated in $k_0 p - \beta p$ diagrams show passbands and stopbands formed in both periodic structures. Those bands are observed for the structures containing six and twenty sections of cylindrical posts in Figs. 16b–16c and 17b–17c, which present the scattering parameters. The number of poles in each band depends on the number of cylindrical sections P and equals P–1.

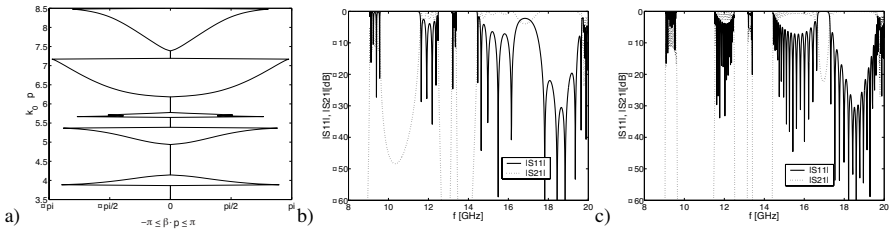

Figure 16. Periodic structure composed of sections of two dielectric cylinders of radii $r_{1,2} = 2\,\text{mm}$; $\varepsilon_{1,2} = 20$; $d_1 = [0, -8]\,\text{mm}$, $d_2 = [0, 8]\,\text{mm}$; period $p = 41\,\text{mm}$; a) $k_0 - \beta$ diagram; b) Frequency responses for six cylindrical sections; c) Frequency responses for twenty cylindrical sections.

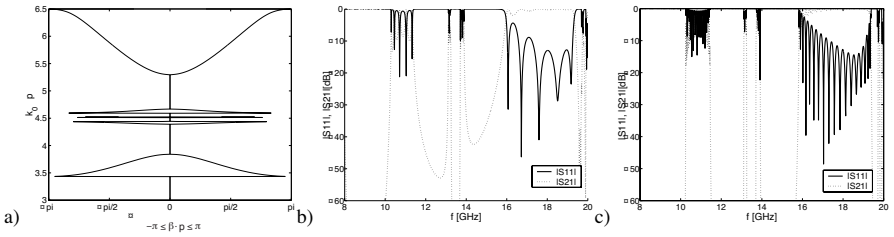

Figure 17. Periodic structure composed of sections of two posts with dielectric rod and three strips. Configuration of the posts: $r_{1,2} = 2\,\text{mm}$; $R_{1,2} = 2.5\,\text{mm}$; $\varepsilon_{1,2} = 25$; $d_1 = [0, -7]\,\text{mm}$, $d_2 = [0, 7]\,\text{mm}$; period $p = 32\,\text{mm}$; a) $k_0 - \beta$ diagram; b) Frequency responses for six cylindrical sections; c) Frequency responses for twenty cylindrical sections.

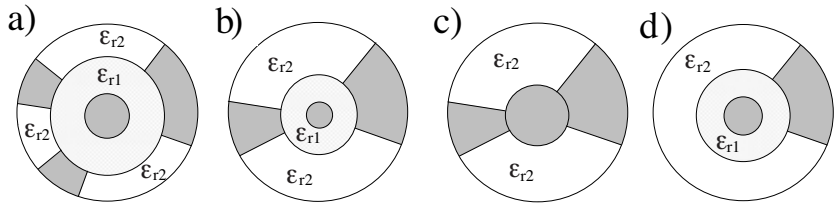

Figure 18. a) Cross section of the propeller post with a dielectric central cylinder b) Cross section of the bow-tie post with a dielectric central cylinder; c) Cross section of the bow-tie post with the conducting central cylinder; d) Cross section of the post with one segment of conducting cylinder.

5. CONCLUSION

The analysis for scattering in an open area and a waveguide junction by a novel structure of a dielectric- metallic post has been developed using a combination of a modified iterative scattering procedure and an orthogonal expansion method. The validity and accuracy of the method have been checked by comparing our results with the ones obtained from the FDTD method and measurements. Our procedure works much faster than the alternative numerical methods (FDTD, FEM). Unlike in FDTD simulator, the computation time is independent of the kind of dielectric material the post is made of. When the dielectric resonators are of high value of ε_r the computation is up to 100 times faster than the calculations of the FDTD simulator.

The displacement, as well as the rotation of a post, vary the electrical characteristic allowing for some adjustments in open structures of the radiation characteristics shape and in waveguide structures of the circuits resonance frequency, making these configurations suitable for tunable filters.

APPENDIX A.

A.1. Dielectric Cylindrical Post with Three Metallic Strips

A cross section of the post with a dielectric rod is presented in Fig. 18a.

A.1.1. Matrices M_{ij} from Equation (19)

$$\begin{aligned} \mathbf{M_{ii}} &= \mathbf{Y_{l_i}^{-1}(k_2 r_2)}\Big(\mathbf{U^{0(i)}L_{ii} - J_{l_i}(k_2 r_2)}\Big) \\ \mathbf{M_{ij}} &= \mathbf{Y_{l_i}^{-1}(k_2 r_2)U^{0(i)}L_{ij}} \end{aligned} \tag{A1}$$

for $i,\ j = 1, 2, 3$. Assuming $p = ((i) \mathrm{mod} I) + 1$, $q = ((i+1) \mathrm{mod} I) + 1$ and $r = (i-j) \mathrm{mod} I$ where $I = max(i)$ (for the propeller cylindrical post $I = 3$) the matrix $\mathbf{L}$ is defined

$$\begin{aligned} \mathbf{L_{ii}} &= \Big(\mathbf{E^{(i,q)} - G^{(q)}A_1^{(i)} + E^{(p,q)}B_1^{(i)}}\Big)^{-1}\Big(\mathbf{G^{(q)}A_2^{(i)} - E^{(p,q)}B_2^{(i)}}\Big) \\ \mathbf{L_{ij}} &= \Big(\mathbf{E^{(i,q)} - G^{(q)}A_1^{(i)} + E^{(p,q)}B_1^{(i)}}\Big)^{-1}\mathbf{C_r^{(i)}} \\ \mathbf{C_1^{(i)}} &= \mathbf{G^{(q)}A_3^{(i)} + E^{(p,q)}B_3^{(i)}} \\ \mathbf{C_2^{(i)}} &= \mathbf{R^{(q)}} \\ \mathbf{A_1^{(i)}} &= \Big(\mathbf{E^{(q,p)} + G^{(p)}\Big(E^{(p,i)}\Big)^{-1}E^{(q,i)}}\Big)^{-1}\Big(\mathbf{G^{(p)}\Big(E_2^{(p,i)}\Big)^{-1}G^{(i)} - E^{(i,p)}}\Big) \\ \mathbf{A_2^{(i)}} &= \Big(\mathbf{E^{(q,p)} + G^{(p)}\Big(E^{(p,i)}\Big)^{-1}E^{(q,i)}}\Big)^{-1}\mathbf{G^{(p)}\Big(E^{(p,i)}\Big)^{-1}R^{(i)}} \\ \mathbf{A_3^{(i)}} &= \Big(\mathbf{E^{(q,p)} + G^{(p)}\Big(E^{(p,i)}\Big)^{-1}E^{(q,i)}}\Big)^{-1}\mathbf{R^{(p)}} \\ \mathbf{B_1^{(i)}} &= \Big(\mathbf{E^{(p,i)}}\Big)^{-1}\Big(\mathbf{G^{(i)} - E^{(q,i)}A_1^{(i)}}\Big) \\ \mathbf{B_2^{(i)}} &= \Big(\mathbf{E^{(p,i)}}\Big)^{-1}\Big(\mathbf{R^{(i)} - E^{(q,i)}A_2^{(i)}}\Big) \\ \mathbf{B_3^{(i)}} &= \Big(\mathbf{E^{(p,i)}}\Big)^{-1}\mathbf{E^{(q,i)}A_3^{(i)}} \end{aligned}$$

and

$$\begin{aligned}
\mathbf{G^{(i)}} &= \mathbf{U^{0(i)T}Y'_{l_i}(k_2r_2)Y^{-1}_{l_i}(k_2r_2)U^{0(i)}} \\
&\quad -\mathbf{U^{\phi(i)T*}X'_m(k_1r_2)X^{-1}_m(k_1r_2)U^{\phi(i)}} \\
\mathbf{R^{(i)}} &= \mathbf{U^{0(p)T}}\Big(\mathbf{J'_{l_i}(k_2r_2) - Y'_{l_i}(k_2r_2)Y^{-1}_{l_i}(k_2r_2)J_{l_i}(k_2r_2)}\Big) \\
\mathbf{E^{(ij)}} &= \mathbf{U^{\phi(j)T*}X'_m(k_1r_2)X^{-1}_m(k_1r_2)U^{\phi(i)}}
\end{aligned}$$

where

$$X_m(k_1\rho) = J_m(k_1\rho) - \frac{J_m(k_1r_1)}{Y_m(k_1r_1)}Y_m(k_1\rho)$$

The matrices $\mathbf{J_{l_i}(kr_2)}$, $\mathbf{Y_{l_i}(kr_2)}$ are diagonal of the dimension $N \times N$, the matrix $\mathbf{X_m(kr_2)}$ is diagonal — $(2M+1) \times (2M+1)$. The matrices $\mathbf{K^{(i)}}$, $\mathbf{G^{(i)}}$ and $\mathbf{E^{(ij)}}$ are square $(K \times K)$, the matrices $\mathbf{L}$, $\mathbf{N^{(i)}}$ and $\mathbf{R^{(i)}}$—$K \times (2M+1)$.

The following notations were introduced for convenience:

$$U^{0(i)}_{nk} = \int_0^{2(\pi-\theta_i)} \frac{\sin\left[\dfrac{k\pi(\phi^i)}{2(\pi-\theta_i)}\right]\sin\left[\dfrac{n\pi\phi^i}{2(\pi-\theta_i)}\right]}{\sqrt[3]{(\phi^i)\left[2(\pi-\theta_i)-(\phi^i)\right]}}d\phi^i \qquad \text{(A2)}$$

$$U^{\phi(i)}_{mk} = e^{-jm\phi_{2i}}\int_0^{2(\pi-\theta_i)} \frac{\sin\left[\dfrac{k\pi(\phi^i)}{2(\pi-\theta_i)}\right]e^{-jm\phi^i}}{\sqrt[3]{(\phi^i)\left[2(\pi-\theta_i)-(\phi^i)\right]}}d\phi^i \qquad \text{(A3)}$$

where $\phi^i = \phi - \phi_i$ for $i = 1,2,3$, $n = 1 \ldots N$, $m = -M \ldots M$, $k = 1 \ldots K$.

A.1.2. Matrices P_{ij}, W_{ij}, Q_i and Q_4 from the Equations (20) and (21)

$$\begin{aligned}
\mathbf{P_{ii}} &= \Big[\Big(\mathbf{J_{l_i}(k_2R) + Y_{l_i}(k_2R)M_{ii}}\Big) + \mathbf{Y_{l_i}(k_2R)M_{iq}O^{(i)}_1} \\
&\quad -\mathbf{Y_{l_i}(k_2R)M_{iq}S_1}\Big]^{-1}\mathbf{U^{0(i)}} \qquad \text{(A4)} \\
\mathbf{P_{ij}} &= \Big[\Big(\mathbf{J_{l_i}(k_2R) + Y_{l_i}(k_2R)M_{ii}}\Big) + \mathbf{Y_{l_i}(k_2R)M_{iq}O^{(i)}_1} \\
&\quad -\mathbf{Y_{l_i}(k_2R)M_{iq}S_1}\Big]^{-1}\mathbf{Y_{l_i}T^{(i)}_r} \qquad \text{(A5)}
\end{aligned}$$

$$\mathbf{W_{ij}} = \sum_{k=1}^{I} \mathbf{M_{ik}} \mathbf{P_{kj}} \tag{A6}$$

$$\mathbf{T_1^{(i)}} = \mathbf{M_{iq}} \mathbf{O_2^{(i)}} - \mathbf{M_{ip}} \mathbf{S_2^{(i)}}$$

$$\mathbf{T_2^{(i)}} = \mathbf{M_{ip}} \mathbf{S_3^{(i)}} - \mathbf{M_{iq}} \mathbf{O_3^{(i)}}$$

$$\mathbf{O_1^{(i)}} = \left[\left(\mathbf{J_{l_q}} + \mathbf{Y_{l_q}} \mathbf{M_{qq}} \right) - \mathbf{Y_{l_q}} \mathbf{M_{qp}} \left(\mathbf{J_{l_p}} + \mathbf{Y_{l_p}} \mathbf{M_{pp}} \right)^{-1} \mathbf{Y_{l_p}} \mathbf{M_{pq}} \right]^{-1} \left(\mathbf{Y_{l_q}} \mathbf{M_{pq}} \left(\mathbf{J_{l_p}} + \mathbf{Y_{l_p}} \mathbf{M_{pp}} \right)^{-1} \mathbf{Y_{l_p}} \mathbf{M_{pi}} - \mathbf{Y_{l_q}} \mathbf{M_{qi}} \right)$$

$$\mathbf{O_2^{(i)}} = \left[\left(\mathbf{J_{l_q}} + \mathbf{Y_{l_q}} \mathbf{M_{qq}} \right) - \mathbf{Y_{l_q}} \mathbf{M_{qp}} \left(\mathbf{J_{l_p}} + \mathbf{Y_{l_p}} \mathbf{M_{pp}} \right)^{-1} \mathbf{Y_{l_p}} \mathbf{M_{pq}} \right]^{-1} \mathbf{Y_{l_q}} \mathbf{M_{pq}} \left(\mathbf{J_{l_p}} + \mathbf{Y_{l_p}} \mathbf{M_{pp}} \right)^{-1} \mathbf{U^{0(p)}}$$

$$\mathbf{O_3^{(i)}} = \left[\left(\mathbf{J_{l_q}} + \mathbf{Y_{l_q}} \mathbf{M_{qq}} \right) - \mathbf{Y_{l_q}} \mathbf{M_{qp}} \left(\mathbf{J_{l_p}} + \mathbf{Y_{l_p}} \mathbf{M_{pp}} \right)^{-1} \mathbf{Y_{l_p}} \mathbf{M_{pq}} \right]^{-1} \mathbf{U^{0(p)}}$$

$$\mathbf{S_1^{(i)}} = \left(\mathbf{J_{l_p}} + \mathbf{Y_{l_p}} \mathbf{M_{pp}} \right)^{-1} \mathbf{Y_{l_p}} \left(\mathbf{M_{pi}} + \mathbf{M_{pq}} \mathbf{O_1^{(i)}} \right)$$

$$\mathbf{S_2^{(i)}} = \left(\mathbf{J_{l_p}} + \mathbf{Y_{l_p}} \mathbf{M_{pp}} \right)^{-1} \left(\mathbf{U^{0(p)}} + \mathbf{Y_{l_p}} \mathbf{M_{pq}} \mathbf{O_2^{(i)}} \right)$$

$$\mathbf{S_3^{(i)}} = \left(\mathbf{J_{l_p}} + \mathbf{Y_{l_p}} \mathbf{M_{pp}} \right)^{-1} \mathbf{Y_{l_p}} \mathbf{M_{pq}} \mathbf{O_3^{(i)}}$$

$$\mathbf{Q_i} = \mathbf{J_m^{-1}}(\mathbf{k_0 R}) \mathbf{U}^{\phi(\mathbf{i})}$$

$$\mathbf{Q_4} = \mathbf{J_m^{-1}}(\mathbf{k_0 R}) \mathbf{H_m^{(2)}}(\mathbf{k_0 R})$$

The matrices $\mathbf{J_{l_i}}(\mathbf{kR})$ and $\mathbf{Y_{l_i}}(\mathbf{kR})$ are diagonal of the dimension $N \times N$, $\mathbf{J_m}(\mathbf{kR})$ and $\mathbf{H_m^{(2)}}(\mathbf{kR})$ are diagonal matrices of the dimension $(2M+1) \times (2M+1)$.

A.1.3. Matrices D from the Equations (23)

$$\mathbf{D_i} = \left[\tilde{\mathbf{G}}^{(\mathbf{i})} - \tilde{\mathbf{E}}^{(\mathbf{p},\mathbf{i})} \mathbf{K_1^{(i)}} - \tilde{\mathbf{E}}^{(\mathbf{q},\mathbf{i})} \mathbf{N_1^{(i)}} \right]^{-1} \left(\tilde{\mathbf{R}}^{(\mathbf{i})} + \tilde{\mathbf{E}}^{(\mathbf{p},\mathbf{i})} \mathbf{K_2^{(i)}} + \tilde{\mathbf{E}}^{(\mathbf{q},\mathbf{i})} \mathbf{N_2^{(i)}} \right) \tag{A7}$$

where

$$\mathbf{K_1^{(i)}} = \left[\tilde{\mathbf{G}}^{(\mathbf{q})} \left(\tilde{\mathbf{E}}^{(\mathbf{q},\mathbf{p})} \right)^{-1} \tilde{\mathbf{G}}^{(\mathbf{p})} - \tilde{\mathbf{E}}^{(\mathbf{p},\mathbf{q})} \right]^{-1} \left(\tilde{\mathbf{G}}^{(\mathbf{q})} \left(\tilde{\mathbf{E}}^{(\mathbf{q},\mathbf{p})} \right)^{-1} \tilde{\mathbf{E}}^{(\mathbf{i},\mathbf{p})} + \tilde{\mathbf{E}}^{(\mathbf{i},\mathbf{q})} \right) \tag{A8}$$

$$\mathbf{K_2^{(i)}} = \left[\tilde{\mathbf{G}}^{(\mathbf{q})}\left(\tilde{\mathbf{E}}^{(\mathbf{q,p})}\right)^{-\mathbf{1}}\tilde{\mathbf{G}}^{(\mathbf{p})} - \tilde{\mathbf{E}}^{(\mathbf{p,q})}\right]^{-\mathbf{1}}\left(\tilde{\mathbf{G}}^{(\mathbf{q})}\left(\tilde{\mathbf{E}}^{(\mathbf{q,p})}\right)^{-\mathbf{1}}\tilde{\mathbf{R}}^{(\mathbf{p})} + \tilde{\mathbf{R}}^{(\mathbf{q})}\right) \tag{A9}$$

$$\mathbf{N_1^{(i)}} = \left(\tilde{\mathbf{E}}^{(\mathbf{q,p})}\right)^{-\mathbf{1}}\left(\tilde{\mathbf{G}}^{(\mathbf{p})}\mathbf{K_1^{(i)}} - \tilde{\mathbf{E}}^{(\mathbf{i,p})}\right) \tag{A10}$$

$$\mathbf{N_2^{(i)}} = \left(\tilde{\mathbf{E}}^{(\mathbf{q,p})}\right)^{-\mathbf{1}}\left(\tilde{\mathbf{G}}^{(\mathbf{p})}\mathbf{K_2^{(i)}} - \tilde{\mathbf{R}}^{(\mathbf{p})}\right) \tag{A11}$$

$$\begin{aligned}
\tilde{\mathbf{G}}^{(\mathbf{i})} &= \mathbf{U^{0(i)T}}\left(\mathbf{J'_{l_i}(k_2R)P_{ii}} + \mathbf{Y'_{l_i}(k_2R)W_{ii}}\right) \\
&\quad -\mathbf{U}^{\phi\mathbf{(i)T*}}\mathbf{J'_m(k_0R)J_m(k_0R)}^{-\mathbf{1}}\mathbf{U}^{\phi\mathbf{(i)}} \\
\tilde{\mathbf{R}}^{(\mathbf{i})} &= -\mathbf{U}^{\phi\mathbf{(i)T*}}\left(\mathbf{J'_m(k_0R)J_m(k_0R)}^{-\mathbf{1}}\mathbf{H_m(k_0R)} - \mathbf{H'_m(k_0R)}\right) \\
\tilde{\mathbf{E}}^{(\mathbf{ij})} &= -\mathbf{U^{0(j)T}}\left(\mathbf{J'_{l_j}(k_2R)P_{ji}} + \mathbf{Y'_{l_j}(k_2R)W_{ji}}\right) \\
&\quad -\mathbf{U}^{\phi\mathbf{(j)T*}}\mathbf{J'_m(k_0R)J_m(k_0R)}^{-\mathbf{1}}\mathbf{U}^{\phi\mathbf{(i)}}
\end{aligned}$$

for $i, j = 1, 2, 3$. The matrices $\mathbf{G^{(i)}}$ and $\mathbf{E^{(i)}}$ are of the dimension K×K, the matrix $\mathbf{R^{(i)}} - \mathbf{K} \times (\mathbf{2M} + \mathbf{1})$.

A.2. Dielectric Cylindrical Post with Two Metallic Strips

For the post structure (see Fig. 18b) there are two sections in Region II_i $(i = 1, 2)$. The equation (19) reduces to:

$$\begin{bmatrix} \mathbf{c^{1'}} \\ \mathbf{c^{2'}} \end{bmatrix} = \begin{bmatrix} \mathbf{M_{11}} & \mathbf{M_{12}} \\ \mathbf{M_{21}} & \mathbf{M_{22}} \end{bmatrix} \begin{bmatrix} \mathbf{c^1} \\ \mathbf{c^2} \end{bmatrix} \tag{A12}$$

The matrices $\mathbf{M}$ are defined similarly to those for the post with three strips (A1) with $I = 2$.

A.3. Metallic Cylindrical Post with Strips

For the conducting central cylinder used in the structure (see Fig. 18c) the fields in Region II_i are independent causing the matrices $\mathbf{M_{ii}}$ form (19) to take diagonal form and $\mathbf{M_{ij}}$ to zero.

$$\mathbf{M_{ii}} = -\mathrm{diag}\left(Y_{l_i}^{-1}(k_2 r_2)J_{l_i}(k_2 r_2)\right)_{m=-M}^{M} \tag{A13}$$

for $i = 1, 2, 3$.

A.4. The Post with Single Metallic Strip

For the single conducting strip attached to the post (see Fig. 18d) the axial component of the electric field in Region II E_z^{II} is described by (12) with $i = 1$. In this connection only the matrix $\mathbf{M_{11}}$ exist in equation (19) describing the relation between unknown coefficients $c^{1'}$ and c^1. For the dielectric central cylinder the matrix $\mathbf{M_{11}}$ is calculated from equation (A1), and for the conducting rod from equation (A13).

REFERENCES

1. Lech, R., M. Polewski, and J. Mazur, "Scattering in junction by posts consisting of a segment of conducting cylinder," *IEEE Transaction on Microwave Theory and Techniques,* Vol. 51, No. 3, 998–1002, March 2003.
2. Polewski, M. and J. Mazur, "Scattering by an array of conducting, lossy dielectric, ferrite and pseudochiral cylinders," *Progress in Electromagnetic Research, PIER* 38, 283–310, 2002.
3. Jim, J. M. and V. V. Liepa, "Application of hybrid finite element method to electromagnetic scattering from coated cylinders," *IEEE Trans. Antennas Propagat.,* Vol. AP-36, 50–54, 1988.
4. Elsherbeni, A. Z. and M. Hamid, "Scattering by parallel conducting circular cylinders," *IEEE Trans. Antennas Propagat.,* Vol. AP-35, 355–358, 1987.
5. Nielsen, E. D., "Scattering by a cylindrical post of complex permittivity in a waveguide," *IEEE Trans. Microwave Theory Tech.,* Vol. 17, 148–153, March 1969.
6. Elsherbeni, A. Z., M. Hamid, and G. Tian, "Iterative scattering of a Gaussian beam by an array of circular conducting and dielectric cylinders," *Journal of Electromagnetic Waves and Applications,* Vol. 7, No. 10, 1323–1342, 1993.
7. Valero, A. and M. Ferrando, "Full-wave equivalent network representation for multiple arbitrary shaped posts in *H*-plane waveguide," *IEEE Transaction on Microwave Theory and Techniques,* Vol. 47, 1997–2002, October 1999.
8. Gesche, R. and N. Löchel, "Two cylindrical obstacles in a rectangular waveguide-resonances and filter applications," *IEEE Transaction on Microwave Theory and Techniques,* Vol. 37, 962–968, June 1989.
9. Gesche, R. and N. Löchel, "Scattering by a lossy dielectric cylinder in a rectangular waveguide," *IEEE Transaction on Microwave Theory and Techniques,* Vol. 36, 137–144, Jan. 1988.

10. Hsu, C. G. and H. A. Auda, "Multiple dielectric posts in a rectangular waveguide," *IEEE Transaction on Microwave Theory and Techniques,* Vol. 34, 883–891, August 1986;
11. Amari, S., S. Catreux, R. Vahldieck, and J. Bornemann, "Analysis of ridged circular waveguides by the coupled-integral-equations technique," *IEEE Transaction on Microwave Theory and Techniques,* Vol. 46, No. 5, May 1998.
12. Ryzyk, I. M. and I. S. Gradsztejn, "Tablice calek, sum, szeregow i iloczynow," *PWN Warszawa,* 1964.
13. Quick-Wave 3D http://www.qwed.com.pl.
14. Amari, S., R. Vahledieck, and J. Bornemann, "Analysis of propagation in periodically loaded circular waveguides," *IEE Proc. — Microw. Antennas Propag.,* Vol. 146, No. 1, February 1999.